

Static adhesion hysteresis in elastic structures

Edvin Memet,¹ Feodor Hilitiski,² Zvonimir Dogic,^{2,3} and L. Mahadevan^{4,*}

¹*Department of Physics, Harvard University, Cambridge, Massachusetts 02138, USA*

²*Department of Physics, Brandeis University, Waltham, Massachusetts 02453, USA*

³*Department of Physics, University of California at Santa Barbara, Santa Barbara, California 93106, USA*

⁴*Paulson School of Engineering and Applied Sciences, Department of Physics, Department of Organismic and Evolutionary Biology, Harvard University, Cambridge, Massachusetts 02138, USA*

(Dated: August 24, 2022)

Adhesive interactions between elastic structures such as graphene sheets, carbon nanotubes, and microtubule axonemes exhibit hysteresis due to irrecoverable energy loss associated with bond breakage, even in static (rate-independent) experiments. Here we provide a simple theory that explains how bond breaking and elastic relaxation can drive static adhesion hysteresis over a debonding/rebonding cycle. We show that energy loss emerges from the coupling of a local event (bond breaking) to a nonlocal event (overall elastic relaxation), in a manner similar to the Lake-Thomas effect in polymers. Experiments with adherent microtubules allow us to quantify the hysteresis as a function of adhesion and elasticity parameters. Our model also helps guide the derivation of a self-consistent continuum boundary condition at the interface of adherent mechanical systems.

The ubiquity of hysteretic behavior in peeling, fracture, or adhesion processes has long been known in systems spanning many orders of magnitude including graphene and carbon nanotubes [1, 2], gecko adhesion [1, 3, 4], actin bundling and dissolution [5], DNA melting and denaturation [6, 7], adhering vesicles [8], partially frayed dynamic axonemes [9], extensile microtubule bundles that generate autonomous flows [10], and elastic contact in soft materials and structures [11–18]. Although it has been nearly a century since Obreimoff measured the energy required to split a multilayer mica sheet [19–21], and interpreted it in terms of an adhesion energy, the microscopic mechanisms behind hysteresis remain incompletely understood. In particular, while hysteresis has been attributed to velocity-dependent processes [20, 22–24], experiments where a thin sheet is peeled from a substrate [1–4, 9, 25–27] show that hysteresis persists even in *static* loading and unloading. Microscopically, normal peeling at high angles is dominated by bending deformations of very stiff filaments, consistent with many recent experiments that explore this mode [1, 4, 9, 28], wherein local elastic deformation of the adhesive bonds is coupled to the nonlocal elastic bending modes of the thin films.

To quantify this, we consider a minimal model consisting of two elastic chains interacting with each other adhesively through reversibly breakable, non-hysteretic springs (Fig. 1A). Each chain has n particles spaced apart by $\Delta l \approx L/n$, where L is the length of a chain. The adhesive interaction is associated with breakable elastic links of stiffness K , rest length y_0 , and cutoff $y_0 + y_c$ that connect corresponding particles on the two chains. One chain is fixed, acting as a rigid foundation, while the other one initially starts in equilibrium and is quasi-statically loaded and unloaded at one end. The potential energy of such a system is given by a sum of filament bending, filament stretching and interfilament adhesion energies and reads

$$\Phi = \frac{1}{2} \left[\sum_{i=2}^{n-1} \frac{B}{\Delta l} (\theta_i - \pi)^2 + \sum_{k=1}^{n-1} k (\mathbf{r}_{\mathbf{k}+1} - \mathbf{r}_{\mathbf{k}} - \Delta l)^2 \right] + \frac{1}{2} \sum_{k=1}^n \min \left(K (\mathbf{r}'_{\mathbf{k}} - \mathbf{r}_{\mathbf{k}})^2, K y_c^2 \right), \quad (1)$$

where the first term represents bending energy defined in terms of the angle θ_i formed by triplets of neighboring particles ($i-1, i, i+1$) along the mobile chain, the second term corresponds to filament stretching, where $\mathbf{r}_{\mathbf{k}} = (x_i, y_i)$, $\mathbf{r}'_{\mathbf{k}} = (x_j, y_j)$ are position vectors for the mobile and fixed chains, respectively, and k is the intra-chain stiffness, while the third term – modeling adhesion – corresponds to stretching the links between chains. In the limit of thin filaments or sheets, the geometric scale separation implies that stretching is very expensive relative to bending, so that we may take the springs connecting particles on the same chain to have a stiffness $k \rightarrow \infty$.

Starting from the energy (1), we can write the overdamped equations of motion for the system as $-\mathbf{d}\Phi/\mathbf{d}\mathbf{r}_{\mathbf{k}} = \gamma_t \dot{\mathbf{r}}_{\mathbf{k}}$ and $-\mathbf{d}\Phi/\mathbf{d}\theta_i = \gamma_r \dot{\theta}_i$, where γ_t and γ_r are translational and rotational damping coefficients. A similar model was proposed nearly fifty years ago [29] to explain lattice trapping of cracks; our results extend this to explain peeling and adhesion hysteresis, and allow us to bridge the discrete-to-continuum gap that has not been addressed before.

Our system is characterized by three length scales: a lattice (discrete) length scale Δl , a maximum displacement associated with adhesive bond breakage y_c , and $l_H \sim (B\Delta l/K)^{1/4}$, a length scale that dictates the size of the transition zone between the peeled and bonded domains [30, 31] and is easiest to recognize in terms of a natural continuum theory for the height profile $y(x)$ inside the bonded region $x > 0$ (Fig. 1A). Indeed, by coarse-graining the discrete energy (1) over length scales large

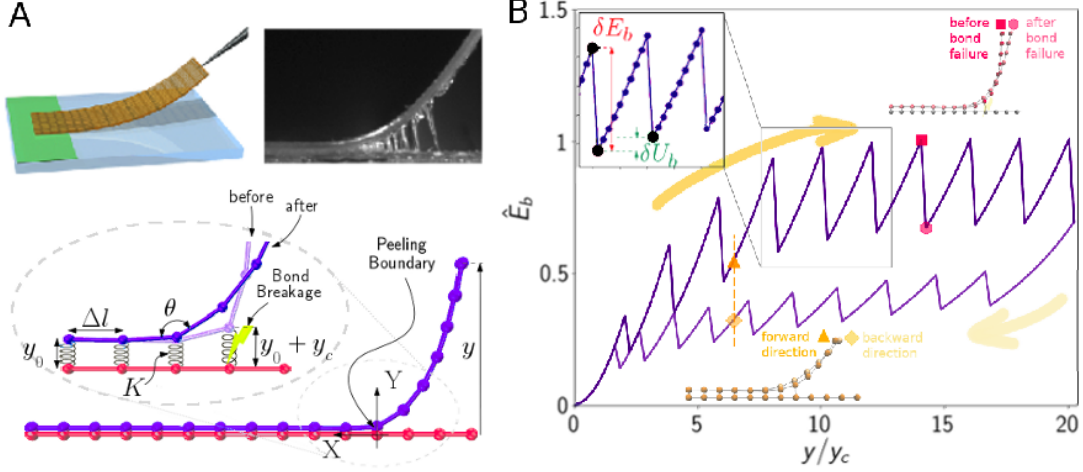


FIG. 1. (A) Top: Representation of peeling graphene sheet (left) and experimental image of peeling a pressure sensitive adhesive (right). Images reproduced from [1] and [27], respectively. Bottom: Discrete elastic chain peeling away from a flat adherent substrate. Zoomed in region illustrates chain and bond rearrangement after bond breakage: as the rightmost bond breaks and moves away from the substrate, remaining bonds stretch more to accommodate the increased stress. (B) Plot of scaled bending energy $\hat{E}_b = E_b/E_b^0$ versus scaled endpoint displacement y/y_c from simulation ($E_b^0 = B\kappa_c^2 l_H = By_c^2/l_H^3$ is the natural scale for bending energy). Arrows indicate the sequence of motion of the free end displacement: first increasing (upper part), then decreasing back to zero (lower part). Filament configurations are represented visually at pairs of points indicated by red and orange symbols, respectively. (Inset): Sawtooth pattern accompanies bond breakage or re-forming. δE_b (red) is the energy loss following single bond breakage, while δU_b (green) is the net bending energy change that accompanies peeling of one segment.

compared to the spacing Δl between bonds, replacing differences by derivatives ($\pi - \theta \rightarrow y'$; $\mathbf{r}'_{\mathbf{k}} - \mathbf{r}_{\mathbf{k}} \rightarrow y(x)$), we find that the Euler-Lagrange equation associated with the continuum version of the functional (1) is

$$By'''' + \frac{K}{\Delta l}y = 0. \quad (2)$$

With boundary conditions $y(\infty) \rightarrow y_0$, $y'(\infty) \rightarrow 0$, $y'''(0) = 0$, and $y(0) \approx y_c$, the solution for $y(x)$ is $y(x) = y_0 + y_{\max} e^{-x/l_H} \cos(x/l_H + \phi)$ [32]. The three length scales generate two independent dimensionless quantities (besides n): $\Delta l/l_H$, which characterizes the mechanical response along the filament direction, and y_c/l_H , which relates to the peeling angle (see SM).

Switching back to the discrete model (Eq. 1), we simulate the corresponding dynamics at zero temperature using Brownian dynamics [33] (see SM for details). We find that when one end of the mobile chain is quasi-statically loaded, bonded segments successively peel from the substrate, while the boundary that separates bonded and debonded phases advances. In the unloading phase, the displacement direction of the free end reverses, causing debonded segments to successively re-enter the interaction range and thus re-adhere to the substrate, leading to healing. The healing pathway is mechanically and thermodynamically different from the peeling pathway, a hallmark of hysteresis. In Fig. 1B, we show that the bending energy-strain plots reveals a characteristic sawtooth pattern arising from alternating elastic loading regimes due to continuous accumulation of the bending

energy and discontinuous debonding transitions between different metastable branches [25, 26]. When a bond breaks, stress redistribution causes it (and the rest of the free chain) to move further away from the range of the adhesive potential (Fig. 1A, inset) such that on its way back it needs to travel more in order to re-form.

Thus, while a single bond does not exhibit hysteresis, the coupling of a local event (bond breaking) to a nonlocal event (overall elastic relaxation), together results in a net energy loss $\delta E < 0$. Indeed, the decrease in bending energy δE_b upon bond breakage (Fig. 1B, inset) is only partially balanced by an increased load on the remaining springs, i.e. an increase in the adhesion energy δE_s . Therefore, the net energy change of the filament is $\delta E = \delta E_b + \delta E_s < 0$ [34]. We expect energy jumps at peeling events δE_b , $\delta E_s \sim E_b^0 \Delta l/l_H \sim Ky_c^2$, with $E_b^0 \equiv B\kappa_c^2 l_H$ being the natural bending energy scale [35].

In the continuum limit, as $\Delta l/l_H \rightarrow 0$ (and $n \rightarrow \infty$), the net energy loss due to the breaking of a single bond must satisfy the limit $\delta E \rightarrow 0$. Since the stress at the free end is accommodated over a scale l_H inside the bonded domain, when $\Delta l \ll l_H$, bond breakage will have a negligible effect on the shape of the peeled filament and thus on the stress distribution. This suggests the following scaling $\delta E \sim Ky_c^2 \times (\Delta l/l_H) \sim E_b^0 \times (\Delta l/l_H)^2$, which is confirmed by simulations (see SM) [36]. To obtain the scaled energy loss due to the breakage of a single bond δe we write $\delta e = \delta E/E_b^0 \sim (\Delta l/l_H)^2$. As we change the discretization n (and the adhesive interaction parameter K along with it), for hysteresis to be independent of

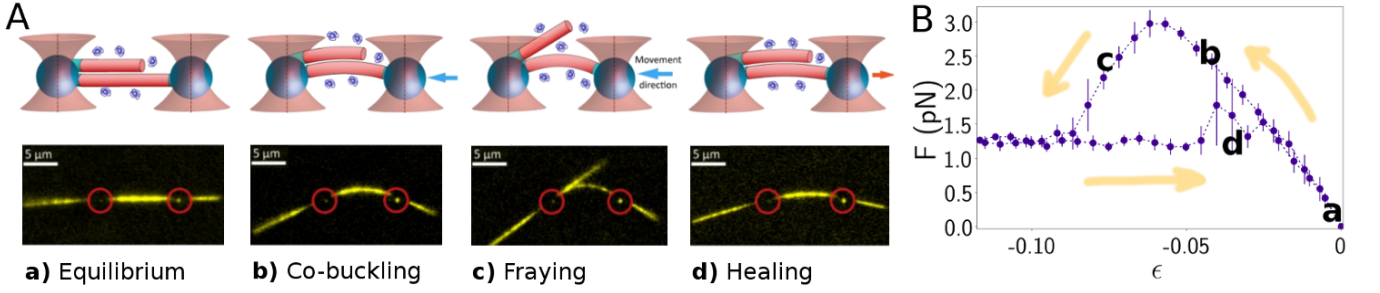


FIG. 2. (A) Fraying of a composite MT bundle in response to a tensile force applied with optical tweezers (bottom) alongside corresponding schematics (top, not to-scale). Red circles indicate trap positions. (B) Measured force-strain exhibited hysteresis associated with bundle fraying and rehealing. Filament configurations corresponding to points (a) to (d) are shown in panel A. Arrows indicate the measured force as the optical trap applies buckling forces and subsequently relaxes back towards the equilibrium. Strain ϵ is defined as $\epsilon = (d - L)/L$, where d is the bead separation and L is the filament length between the two attachment points.

discretization, the scaled energy loss summed across all segments, $n\delta e \sim n(\Delta l/l_H)^2$, and the adhesion energy per unit length, $J = nKy_c^2/L$, must remain invariant. Substituting $K = JL/(ny_c^2)$ in the expression for $n\delta e$ and recognizing that $l_H \sim [BL/(nK)]^{1/4}$, we find that

$$n\delta e \sim \frac{L^2}{ny_c} \left(\frac{J}{B} \right)^{1/2}. \quad (3)$$

Invariance of the energy loss $n\delta e$ in the continuum limit implies $y_c \sim 1/n$, while invariance of J requires that $K \sim n$. As a result, $l_H \sim (nK)^{-1/4} \sim 1/\sqrt{n}$, which means that in the continuum limit the transition between the bonded and debonded regions occurs instantly, with $l_H \rightarrow 0$, without a weakly bound intermediate region.

Our findings allow us to immediately explain recent experiments reporting very large hysteresis in peeling graphene [1] as deriving from the this local-global elastic coupling (see SM). To further test this theory we turn to new experiments involving a pair of microtubules (MTs) held together by the depletion interaction, induced by addition of non-adsorbing polymers. The range and strength of the tunable depletion attraction between the filaments is determined respectively by the size and the concentration of the polymer.[37, 38]

To obtain such a system, micron-sized silica beads are attached with optical tweezers at two points along a single MT as described elsewhere [39]. Next, a shorter MT is attached to the longer filament by the depletion interaction and is linked to one bead by the biotin-streptavidin linkage (Fig. 2A). The mobile optical traps were displaced quasi-statically, subjecting the composite bundle to buckling forces that were measured using conventional techniques [39]. While the adhering MTs initially buckle together, above a critical strain the free end of the shorter MT begins to detach (“fray”). Further increasing strain, leads to almost complete peeling of the shorter MT (Fig. 2A). From this point on, only the longer

MT contributes to the buckling force, which is roughly independent of strain due to the effective softening induced by cross-sectional flattening [39, 40]. Reversing optical trap displacement reduces strain, eventually leading to re-adhesion, albeit at smaller curvatures/strains than for peeling. Hysteresis is apparent in the force-strain curves associated with this measurement, where strain $\epsilon = (d - L)/L$ (Fig. 2B).

Compared to peeling from a flat substrate, the microtubule system exhibits added complexity, as both microtubules are allowed to bend. Consequently, we need to revisit the theory, generalizing it for flexible substrates. Towards that end, we examine an elastic chain model in which both filaments are mobile and we can apply a buckling force at one end, through a bead attached to the longer filament (Fig. 3A). Letting functions $\kappa(s)$ and $\kappa'(s)$ characterize the curvatures of the two filaments, previous results still hold, but for relative curvature $\kappa_r(s) = |\kappa(s) - \kappa'(s)|$, whose maximal value κ_c determines the onset of fraying. Previously, $\kappa' = 0$, $\kappa_r = \kappa$ and the bending energy scale could be expressed in terms of κ_c : $E_b^0 \sim B\kappa_c^2 l_H$. Here, the analogous quantity is a “relative” bending energy $\tilde{E}_b^0 \sim B\kappa_c^2 l_H$, while the proper bending energy scale is $E_b^0(\kappa, \kappa') = B/L$ (force B/L^2 times length L).

We now assume, in analogy with results from our first model, that the net energy loss $\delta E \sim B\kappa_c^2 l_H \times (\Delta l/l_H)^2$. Expressing the total scaled energy loss $n\delta e = n\delta E/E_b^0$ in terms of adhesion energy per unit length J , we get

$$n\delta e \sim \frac{L}{ny_c^{1/2}} \left(\frac{J}{B} \right)^{1/4} (\kappa_c L)^2, \quad (4)$$

where J and κ_c are invariants. This invariance implies $y_c \sim 1/n^2$, $K \sim n^3$. Simulations (using the same molecular dynamics setup as in the 1D model in [39] and adding a second filament and a breakable adhesive interaction between corresponding beads on each filament – see SM

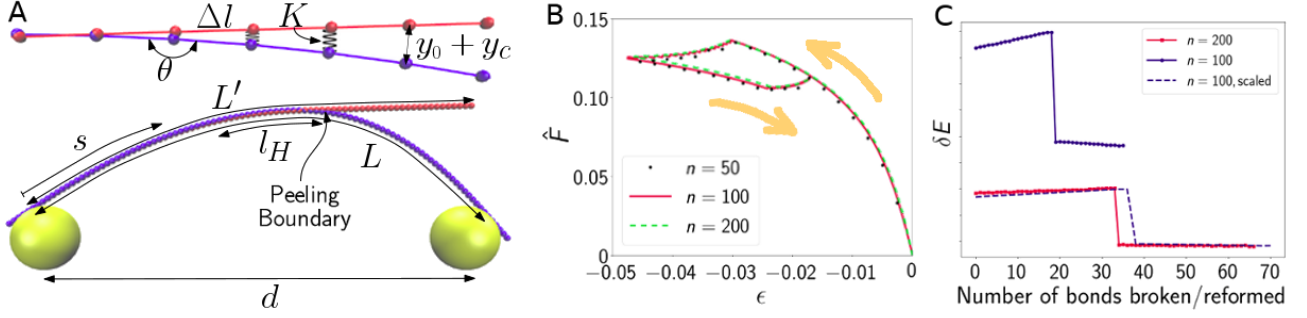


FIG. 3. (A) Generalized elastic chain model in which both filaments are free to deform. The longer filament (blue) is attached rigidly to two optical beads (yellow), while the shorter, adhering filament (red) is attached to only one bead. The right optical bead is mobile, while the left one is fixed. (B) Scaled force $\bar{F} = F / (B/L^2)$ plotted as a function of imposed strain ϵ for three simulations with parameter scaling as $K \rightarrow n^3 K$, $y_c \rightarrow y_c/n^2$. (C) Energy loss per bond broken or re-formed versus the cumulative number of bonds broken/re-formed for two of the simulations in panel B, with $n = 100$ (blue) and $n = 200$ (red). The two profiles can be made to collapse (signifying equal scaled hysteresis size) by scaling the horizontal axis by a factor of Δl and the vertical axis by the bending energy scale E_b^0 .

for details) confirm that the scaling forms $K \rightarrow n^3 K$ and $y_c \rightarrow y_c/n^2$ preserve hysteresis [41] (Fig. 3B, 3C). Previous measurements indicate that $J \sim 0.1$ pN for MT depletion-induced cohesion [38], which allows us to reproduce both the onset of fraying and approximate hysteresis size (Fig. 4, green). To better capture the experimental hysteresis curve, we need to include factors such as the cross-sectional flattening of MTs [39] and the hysteresis-narrowing effect of thermal fluctuations (see SM).

Interestingly, hysteresis in the graphene peeling experiments [1] is significantly larger than in the microtubule experiments. To understand how this observation fits in the context of our predictions, consider Eqs. (3) and (4) – equivalently, Eqs. (S.5) and (S.6) in the SM – expressing scaled hysteresis in the graphene and microtubule settings, respectively. We note that, although the scaling exponents for the graphene and microtubule cases differ, hysteresis in both cases is proportional to the adhesive length L and inversely proportional to y_c and $\sqrt{B/J}$. While $\sqrt{B/J}$ is comparable between the two experiments, the adhesive interaction in the graphene experiments is much shorter range ($y_c \sim 0.1$ nm) than the depletion-mediated interaction in MT experiments ($y_c \sim 10$ nm). Therefore, the very large hysteresis observed in graphene peeling experiments is consistent with our model (see SM for more details).

In summary, we have shown that in a simple model of peeling adhesion hysteresis arises due to energy lost at transitions between metastable states [25, 26], a result that is preserved in the continuum limit. This is similar to a phenomenon in polymer fracture known as the Lake-Thomas effect [42, 43], wherein the energy required to rupture an elastomer is much larger than the energy to break all the typical density of chains crossing the fracture plane [44], due to the energy loss when the stretched chains away from the fracture zone relax as the crack propagates [3, 44–48]. This notion of stretching globally

while breaking locally can also be observed in our model, where at a given moment the adhesive bonds within a region of size l_H are stretched whereas upon peeling or healing, energy is released from a single spring, spanning a region of size Δl . The difference, however, is that in our case when a bond breaks, it does not result in relaxing the strain energy over the entire region that is under stress, as is the case with fracture.

Additionally, we have derived a simple way of scaling adhesive parameters K and y_c with discretization n in order to preserve hysteresis with coarse- or fine-graining a continuum system, both in peeling from a flat and from a flexible substrate. Counter-intuitively, our results also imply that, for a given n , there exists a single,

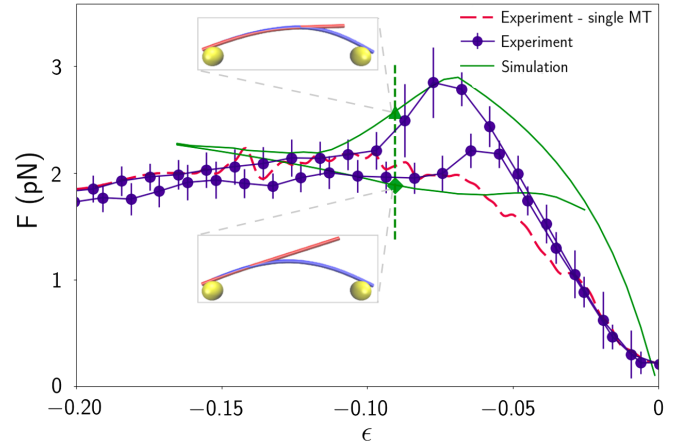


FIG. 4. (A) Measured force versus strain (blue) for a MT bundle composed of two MTs ($8.2 \mu\text{m}$ and $5.6 \mu\text{m}$). The buckling curve of the longer microtubule alone is shown in red. Simulation results are shown in green ($B = 19 \text{ pN } \mu\text{m}^2$, $n = 100$, $K = 40 \text{ pN}/\mu\text{m}$, and $y_c = 0.02 \mu\text{m}$) with filament configurations shown at two points of equal strain (green symbols).

well-defined choice of the adhesion parameters K and y_c (see SM) [49]. Our results should prove very useful in facilitating the modeling and simulation of many quasi-continuum systems that can exhibit adhesion hysteresis.

We thank the Department of Energy - Basic Energy Sciences grant DE-SC0019733, the Brandeis MRSEC biological and optical microscopy facilities NSF-1420382, and NSF DMR 14-20570 MRSEC, and NSF DMR 15-33985 Biomatter for partial financial support.

* lmahadev@g.harvard.edu

- [1] M. Z. Miskin, C. Sun, I. Cohen, W. R. Dichtel, and P. L. McEuen, *Nano letters* **18**, 449 (2017).
- [2] N. Sasaki, A. Toyoda, N. Itamura, and K. Miura, *e-J Surf Sci Nanotechnol* **6**, 72 (2008).
- [3] Y. Chen, C. Helm, and J. Israelachvili, *J. Phys. Chem.* **95**, 10736 (1991).
- [4] Y. Sekiguchi, P. Hemthavy, S. Saito, and K. Takahashi, *Int. J. Adhes. Adhes.* **49**, 1 (2014).
- [5] M. Hosek and J. Tang, *Phys. Rev. E* **69**, 051907 (2004).
- [6] N. Bosaeus, A. H. El-Sagheer, T. Brown, B. Åkerman, and B. Nordén, *Nucleic Acids Res.* **42**, 8083 (2014).
- [7] M. Peyrard, *Nonlinearity* **17**, R1 (2004).
- [8] M. Dembo, D. Torney, K. Saxman, and D. Hammer, *Proc. R. Soc. Lond. B* **234**, 55 (1988).
- [9] S. Aoyama and R. Kamiya, *Biophys. J.* **89**, 3261 (2005).
- [10] T. Sanchez, D. T. Chen, S. J. DeCamp, M. Heymann, and Z. Dogic, *Nature* **491**, 431 (2012).
- [11] D. Maugis, *Contact, adhesion and rupture of elastic solids*, Vol. 130 (Springer, 2013).
- [12] N. S. Pesika, Y. Tian, B. Zhao, K. Rosenberg, H. Zeng, P. McGuiggan, K. Autumn, and J. N. Israelachvili, *J. Adhes.* **83**, 383 (2007).
- [13] C. Majidi and G. G. Adams, in *Proc. R. Soc. Lond. A*, Vol. 465 (2009) pp. 2217–2230.
- [14] A. Molinari and G. Ravichandran, *J. Adhes.* **84**, 961 (2008).
- [15] T. Cohen, C. U. Chan, and L. Mahadevan, *Soft matter* **14**, 1771 (2018).
- [16] M. Kamperman, E. Kroner, A. del Campo, R. M. McMeeking, and E. Arzt, *Adv. Eng. Mater.* **12**, 335 (2010).
- [17] J. A. Williams, *J. Phys. D: Appl. Phys.* **48**, 015401 (2014).
- [18] X. Oyharcabal and T. Frisch, *Phys. Rev. E* **71**, 036611 (2005).
- [19] J. Obreimoff, *Proc. R. Soc. Lond. A* **127**, 290 (1930).
- [20] K. Kendall, *Molecular adhesion and its applications: the sticky universe* (Springer, 2007).
- [21] A. V. Pocius and D. A. Dillard, *Adhesion science and engineering: surfaces, chemistry and applications* (Elsevier, 2002).
- [22] Z. Liu, H. Lu, Y. Zheng, D. Tao, Y. Meng, and Y. Tian, *Sci. reports* **8**, 6147 (2018).
- [23] J. Y. Chung and M. K. Chaudhury, *J. R. Soc. Interface* **2**, 55 (2005).
- [24] V. De Zotti, K. Rapina, P.-P. Cortet, L. Vanel, and S. Santucci, *Phys. Rev. Lett.* **122**, 068005 (2019).
- [25] G. Puglisi and L. Truskinovsky, *Phys. Rev. E* **87**, 032714 (2013).
- [26] F. Maddalena, D. Percivale, G. Puglisi, and L. Truskinovsky, *Cont. Mech. Therm.* **21**, 251 (2009).
- [27] R. Villey, C. Creton, P.-P. Cortet, M.-J. Dalbe, T. Jet, B. Saintyves, S. Santucci, L. Vanel, D. J. Yarusso, and M. Ciccotti, *Soft Matter* **11**, 3480 (2015).
- [28] B. Zhao, H. Zeng, Y. Tian, and J. Israelachvili, *PNAS* **103**, 19624 (2006).
- [29] R. Thomson, C. Hsieh, and V. Rana, *J. Appl. Phys.* **42**, 3154 (1971).
- [30] S. Zapperi and L. Mahadevan, *Biophys. J.* **101**, 267 (2011).
- [31] I. M. Jánosi, D. Chrétien, and H. Flyvbjerg, *Eur. Biophys. J.* **27**, 501 (1998).
- [32] The curvature at the peeling boundary is $\kappa_c = y''(0) \approx 2y_c/l_H^2 \tan(\phi) = \kappa_c^{\text{pred}} \tan(\phi)$, where $\kappa_c^{\text{pred}} = 2y_c/l_H^2$ corresponds to the value used in the continuum elasticity literature [13, 50, 51]. However, we find that generally the factor $\tan(\phi) = \kappa_c/\kappa_c^{\text{pred}} \neq 1$ so that $\kappa_c \neq \kappa_c^{\text{pred}}$.
- [33] A. Arnold, O. Lenz, S. Kesselheim, R. Weeber, F. Fahrenberger, D. Roehm, P. Košovan, and C. Holm, in *Meshfree Methods for Partial Differential Equations VI* (Springer, 2013) pp. 1–23.
- [34] When a bond reforms, $\delta E_b > 0$ and $\delta E_s < 0$ such that there is still net energy dissipation $\delta E < 0$.
- [35] The same scaling also applies to δU_b , the net bending energy change corresponding to peeling a single segment (Fig. 1B, inset). Intuitively, $\delta U_b \sim B\kappa_c^2 \Delta l \sim B\kappa_c^2 l_H \times (\Delta l/l_H) E_b^0 \Delta l/l_H$.
- [36] Interestingly, in going from E_b to δE_b (the difference of two envelope functions E_b^+ and E_b^- going through the maxima/minima of the sawtooth pattern, respectively) and finally to δE (the difference between the magnitudes of δE_b and δE_d) we tack on successive factors of $\Delta l/l_H$.
- [37] S. Asakura and F. Oosawa, *J. Chem. Phys.* **22**, 1255 (1954).
- [38] F. Hilitski, A. R. Ward, L. Cajamarca, M. F. Hagan, G. M. Grason, and Z. Dogic, *Phys. Rev. Lett.* **114**, 138102 (2015).
- [39] E. Memet, F. Hilitski, M. A. Morris, W. J. Schwenger, Z. Dogic, and L. Mahadevan, *eLife* **7**, e34695 (2018).
- [40] R. A. Cross, *Curr. Opin. Cell Biol.* **56**, 88 (2019).
- [41] Provided we adjust the length of the shorter filament to account for the changing healing length $l_H \sim 1/n$, since the filaments are weakly bonded over this length scale.
- [42] G. Lake and A. Thomas, *Proc. R. Soc. Lond. A* **300**, 108 (1967).
- [43] S. Wang, S. Panyukov, M. Rubinstein, and S. L. Craig, *Macromolecules* **52**, 2772 (2019).
- [44] C.-Y. Hui, A. Jagota, S. Bennison, and J. Londono, in *Proc. R. Soc. Lond. A*, Vol. 459 (2003) pp. 1489–1516.
- [45] X. Zhao, *Soft Matter* **10**, 672 (2014).
- [46] C. Creton and M. Ciccotti, *Rep. Prog. Phys.* **79**, 046601 (2016).
- [47] E. Andrews, T. Khan, and N. Lockington, *J. Mater. Sci.* **22**, 2833 (1987).
- [48] H. R. Brown, *Macromolecules* **40**, 3815 (2007).
- [49] The fact that the cutoff length y_c changes with n rather than being fixed at the actual cutoff of the adhesion potential is also counterintuitive, and thus easily overlooked.
- [50] M. Stewart, A. D. McLachlan, and C. R. Calladine, *Proc. R. Soc. Lond. B* **229**, 381 (1987).
- [51] C. Majidi, O. M. O'Reilly, and J. A. Williams, *J. Mech.*

Phys. Sol. **60**, 827 (2012).